
The trade-off between long-term memory and smoothness for recurrent networks

Antônio H. Ribeiro*

Graduate Program in Electrical Engineering
Universidade Federal de Minas Gerais
Belo Horizonte, Brazil
antonio-ribeiro@ufmg.br

Koen Tiels

Department of Information Technology
Uppsala University
Sweden
koen.tiels@it.uu.se

Luis A. Aguirre

Department of Electronic Engineering
Universidade Federal de Minas Gerais
Belo Horizonte, Brazil
aguirre@ufmg.br

Thomas B. Schön

Department of Information Technology
Uppsala University
Sweden
thomas.schon@it.uu.se

Abstract

Training recurrent neural networks (RNNs) that possess long-term memory is challenging. We provide insight into the trade-off between the smoothness of the cost function and the memory retention capabilities of the network. We express both aspects in terms of the Lipschitz constant of the dynamics modeled by the network. This allows us to make a distinction between three types of regions in the parameter space. In the first region, the network experiences problems in retaining long-term information, while at the same time the cost function is smooth and easy for gradient descent to navigate in. In the second region, the amount of stored information increases with time and the cost function is intricate and full of local minima. The third region is in between the two other regions and here the RNN is able to retain long-term information. Based on these theoretical findings we present the hypothesis that good parameter choices for the RNN are located in between the well-behaved and the ill-behaved cost function regions. The concepts presented in the paper are illustrated by artificially generated and real examples.

1 Introduction

Recurrent neural networks (RNNs) have previously been the *de facto* state-of-the-art on a number of machine learning tasks, but they are now being challenged by new, high performance, feedforward network structures. These include the transformer architecture [1] and causal convolutional networks [2], which yield impressive results in language and music modeling [2–6], text-to-speech conversion [3], machine translation [7, 8] and other sequential tasks [2].

This shift of paradigm requires understanding of the limitations and challenges in training RNNs. It is well-known that learning long-term dependencies with gradient descent is difficult [9–11]. While long short-term memory (LSTM) [12] and gated recurrent unit (GRU) [13] networks have been designed to capture these dependencies, we argue that there are still great challenges in training such models.

*Work performed while at Uppsala University as a visiting Ph.D. Student in the Department of Information Technology.

Dynamic system analysis has been a major tool in understanding the challenges in training RNNs [14, 9–11, 15, 16]. In this paper we use dynamic system theory to analyze two different aspects of RNN training and usage: the cost function smoothness and the capability of retaining information. We show that there is indeed a direct relationship between these two aspects.

We have three main contributions. The first contribution is a novel theoretical result on the smoothness of the cost function (Section 3). We divide the parameter space into three regions for which the Lipschitz constant of the cost function scales: i) as a constant; ii) as a polynomial; or, iii) exponentially with the simulation length. Region (ii) constitutes the boundary between the two other regions. Using examples we show that it might be very hard for derivative-based (i.e. gradient descent) algorithms to navigate in region (iii).

The second contribution is an information-theoretic approach for quantifying the amount of information stored in an RNN (Section 4). We present a lower bound on the amount of information, expressed in terms of entropy, and show that the three different behaviors of the cost function correspond to regimes for which the RNN entropy: i) possibly decreases; ii) is retained; iii) increases.

The third contribution is the hypothesis that the solutions for which the RNN present "long-term" memory can be found close to region (ii), on the boundary between the well-behaved and ill-behaved cost function regions. This hypothesis might be the origin of many of the difficulties that arise in training RNNs.

2 Background on RNNs and long-term memory

RNNs are non-linear discrete-time dynamical systems:

$$\mathbf{x}_{t+1} = \mathbf{f}(\mathbf{x}_t, \mathbf{u}_t; \boldsymbol{\theta}), \quad (1a)$$

$$\hat{\mathbf{y}}_t = \mathbf{g}(\mathbf{x}_t, \mathbf{u}_t; \boldsymbol{\theta}), \quad (1b)$$

with input $\mathbf{u}_t \in \mathbb{R}^{N_u}$, hidden state $\mathbf{x}_t \in \mathbb{R}^{N_x}$, predicted output $\hat{\mathbf{y}}_t \in \mathbb{R}^{N_y}$, and parameters $\boldsymbol{\theta}$. This representation is sufficiently general to capture vanilla RNNs, LSTM [12], GRU [13] and stacked layers of these units.

For a given training sequence $\mathcal{Z}^N = \{(\mathbf{u}_t, \mathbf{y}_t), t = 1, 2, \dots, N\}$, a cost function can be defined:

$$V = \frac{1}{N} \sum_{t=1}^N l(\mathbf{y}_t, \hat{\mathbf{y}}_t). \quad (2)$$

The parameter vector $\boldsymbol{\theta}$ is estimated (i.e. the neural network is trained) by minimizing V or, for the case of multiple independent training sequences, minimizing a weighted average of many V 's defined as above. Here, l is the loss function. Common choices for regression and classification problems are the squared error and cross entropy loss, respectively.

In what follows, the concept of long-term memory will be closely related to the definition of an attractor of a dynamical system. Similar approaches have been pursued in [9, 10].

Definition 1 (attractor of a dynamical system). Let \mathbf{u}_t be equal to a constant $\bar{\mathbf{u}}$ for every t . An **attractor** of a dynamical system:

$$\mathbf{x}_{t+1} = \mathbf{f}(\mathbf{x}_t, \bar{\mathbf{u}}; \boldsymbol{\theta}), \quad (3)$$

is a subset $A \in \mathbb{R}^{N_x}$ for which:

1. if $\mathbf{x}_{t_0} \in A$ then $\mathbf{x}_t \in A$ for all $t \geq t_0$;
2. there exists a neighborhood of A , called **basin of attraction** $B(A)$, such that for any open neighborhood of A , say N , there is a positive integer $T \geq t_0$ such that if $\mathbf{x}_{t_0} \in B(A)$ then $\mathbf{x}_t \in N$ for all real $t > T$;
3. there is no proper (non-empty) subset of A having the first two properties.

Property 1 is related to the concept of long-term memory. If at a given time instant t_0 , $\mathbf{x}_{t_0} \in A$, the system state will still be in A at any point in the future, that is, it will "remember" this set A . Systems that do not respect this property will just leave (i.e. "forget") set A for some $t > t_0$.

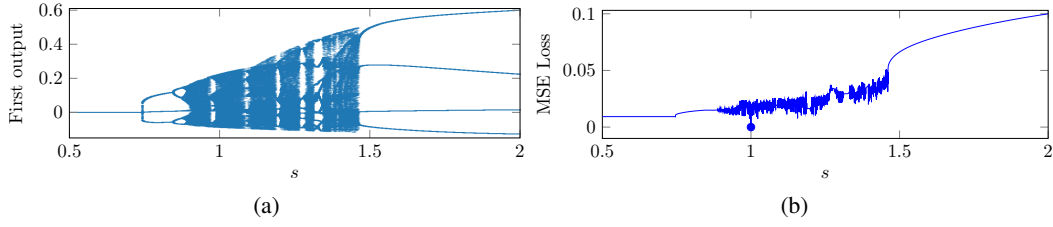


Figure 1: (**chaotic LSTM**) Bifurcation diagram (a) and mean-square cost function (b) for LSTM models with parameter vectors $\theta(s) = s\theta_{\text{true}}$.

Property 2 is related to the robustness of the long-term memory. If a given state \mathbf{x}_t belongs to $B(A)$ then $\mathbf{x}_t \rightarrow A$ as $t \rightarrow \infty$. If we apply a finite non-zero input sequence \mathbf{u} sufficiently small such that the state remains in $B(A)$, then for \mathbf{f} continuous in \mathbf{u} the system will converge to A . In other words, the system will not “forget” A even in the presence of some (sufficiently small) disturbance.

In the numerical examples of this paper we use the **bifurcation diagram** for visualizing the attractors of the RNN. These diagrams show the values visited in steady state behavior (when a constant input is applied to the system) as a function of some bifurcation parameter s . See Figure 1 (a).

3 Smoothness of the cost function

In this section, we relate the *smoothness* of the cost function to the dynamics of the RNN. Our analysis is based on the Lipschitz constant of the cost function and on the Lipschitz constant of the cost function gradient (sometimes called β -smoothness). Both constants play a crucial role in optimization [17] and can be understood as qualitative measurements of how *smooth* the cost function is. Lower values imply that the cost function is less intricate and that optimization algorithms can still converge while taking larger steps. It also provides an upper bound on how distinct in performance two close local minima may be.

In Section 3.1, we discuss an example of an LSTM model that exhibits chaotic behavior for certain parameter values. Chaotic systems have *infinitely* long memory in the sense that modifications in the state of the system, no matter how small and how far back into the past, yield different trajectories. We show that the cost function is intricate in the same region of the parameters space for which the system displays chaotic behavior. This indicates that there is a correspondence between long-term memory effects (like chaos) and *smoothness* of the cost function. This serves as motivation for the more theoretical investigation carried out in Section 3.2.

3.1 Motivating example – Chaotic LSTM

This example considers an LSTM model with zero input and without bias terms. The outputs of the model are the sequences of the two hidden states. Sequences of 200 samples are simulated starting from fixed non-zero initial conditions and for a fixed set of parameters that result in chaotic behavior. The first 100 samples are discarded to remove the transient. Further details on the parameter values can be found in Appendix A.1.

Figure 1(b) shows the mean-square loss for LSTM models with parameters interpolated (and extrapolated) between zero and those used to generate the data, i.e. for LSTM models with parameter vectors $\theta(s) = s\theta_{\text{true}}$. The cost function is intricate in an entire region around the data-generating parameter values ($s = 1$). Figure 1 (a) shows the last 100 samples of the first output as a function of the interpolation parameter s . We see that the data-generating parameters correspond to a chaotic attractor. Comparing with the cost function in Figure (b), we observe that the region in parameter space where the cost function is intricate ($0.9 \lesssim s \lesssim 1.45$) corresponds to the region where the LSTM shows interesting behavior (limit cycles or chaotic attractors). An evaluation of the cost function on a two-dimensional grid is available in Appendix A.1 and it also shows many neighboring local minima in an entire region around θ_{true} .

3.2 Theoretical Results

The theorem below relates the Lipschitz constant of the cost function V and of its gradient (i.e. β -smoothness) to the simulation length N . This extends the results we presented in [18].

Theorem 1 (Lipschitz constants of V and ∇V). *Let $\mathbf{f}(\mathbf{x}, \mathbf{u}; \boldsymbol{\theta})$ and $\mathbf{g}(\mathbf{x}, \mathbf{u}; \boldsymbol{\theta})$ in Eq. (1) be Lipschitz in $(\mathbf{x}, \boldsymbol{\theta})$ with constants L_f and L_g on a compact and convex set $\Omega = (\Omega_{\mathbf{x}}, \Omega_{\mathbf{u}}, \Omega_{\boldsymbol{\theta}})$. Assume the loss function is either $l(\hat{\mathbf{y}}, \mathbf{y}) = \|\mathbf{y} - \hat{\mathbf{y}}\|^2$ or $l(\hat{\mathbf{y}}, \mathbf{y}) = -\mathbf{y}^T \log(\sigma(\hat{\mathbf{y}})) - (1 - \mathbf{y})^T \log(1 - \sigma(\hat{\mathbf{y}}))$. With $\{\mathbf{u}_t\}_{k=1}^N \subseteq \Omega_{\mathbf{u}}$ and $(\Omega_{\mathbf{x}}, \Omega_{\boldsymbol{\theta}}) \subseteq \mathbb{R}^{N_{\theta}}$. If there exists at least one choice of $(\mathbf{x}_0, \boldsymbol{\theta})$ for which there is an invariant set contained in Ω , then, for trajectories and parameters confined within Ω :*

1. *The cost function V defined in (2) is Lipschitz with constant:*²

$$L_V = \begin{cases} \mathcal{O}(L_f^{2N}) & \text{if } L_f > 1, \\ \mathcal{O}(N) & \text{if } L_f = 1, \\ \mathcal{O}(1) & \text{if } L_f < 1. \end{cases} \quad (4)$$

2. *If the Jacobian matrices of \mathbf{f} and \mathbf{g} are also Lipschitz with respect to $(\mathbf{x}, \boldsymbol{\theta})$ on Ω , then the gradient of the cost function ∇V is also Lipschitz with constant:*

$$L'_V = \begin{cases} \mathcal{O}(L_f^{3N}) & \text{if } L_f > 1, \\ \mathcal{O}(N^3) & \text{if } L_f = 1, \\ \mathcal{O}(1) & \text{if } L_f < 1. \end{cases} \quad (5)$$

Proof. In Appendix C. □

Remark (other loss functions). *The above theorem was stated for two different loss functions (squared error and average cross entropy preceded by the sigmoid function). The theorem still holds for any loss function for which the equivalent of Lemma 2 (see Appendix C) remains true.*

For better understanding of Theorem 1, it is interesting to have the concept of a contractive system in mind:

Definition 2 (contractive system). *We say the dynamical system (3) is contractive in $\Omega_{\mathbf{x}}$ if, for all \mathbf{x} and \mathbf{w} in $\Omega_{\mathbf{x}}$, it satisfies:*

$$\|\mathbf{f}(\mathbf{x}, \bar{\mathbf{u}}; \boldsymbol{\theta}) - \mathbf{f}(\mathbf{w}, \bar{\mathbf{u}}; \boldsymbol{\theta})\| < L_{\bar{\mathbf{u}}} \|\mathbf{x} - \mathbf{w}\|, \quad \text{for } L_{\bar{\mathbf{u}}} < 1. \quad (6)$$

If the system is not contractive: $L_f \geq 1^3$. All contractive systems have a unique fixed point inside the contractive region, and all trajectories converge to such a fixed point [19, Theorem 9.23], hence systems with richer nonlinear dynamic behaviors, such as multiple fixed points, limit cycles and chaotic attractors, and also unstable systems, are *non-contractive* and will always have $L_f \geq 1$. The Lipschitz constants and β -smoothness for these systems may, according to Theorem 1, blow up exponentially (or polynomially for some limit cases) with the maximum simulation length. This results in very intricate cost functions, see Figure 1 (b).

Long-term dependencies are deeply related to the concept of attractors (see Section 2). Models that are contractive, after a sufficiently long time, will remember only a single point of information, since all solutions will converge to a single point. Models that remember more than a single bit of long-term information (i.e. have an attractor that is not only a single point) are inherently non-contractive. According to Theorem 1, however, these interesting regions for which the system is non-contractive, might have very intricate cost functions, full of local minima and for which low-order (Taylor) approximations of the cost function might be very inaccurate.

4 Gauging the information in an RNN

The previous section introduced the limitation of a contractive system: after a sufficiently long time all trajectories converge to a single point and that is all the information the dynamic system will

²Here \mathcal{O} is the big O notation. It should be read as: $L(N) = \mathcal{O}(g(N))$ if and only if there exist positive integers M and N_0 such that $|L(N)| \leq M g(N)$ for all $N \geq N_0$.

³If $\bar{\mathbf{u}} \in \Omega_{\mathbf{u}}$ it follows that $L_f \geq L_{\bar{\mathbf{u}}}$, hence if the system is not contractive $L_f \geq L_{\bar{\mathbf{u}}} \geq 1$.

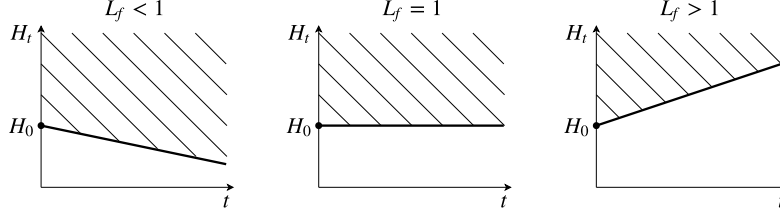


Figure 2: Illustration of the lower bound on the entropy H_t obtained in (9). Starting from H_0 , the entropy H_t can only take values in the shaded region. The entropy can decay over time when $L_f < 1$ (contractive system), can remain constant when $L_f = 1$ (e.g. for a periodic oscillator), and increases when $L_f > 1$ (e.g. for a chaotic system).

actually store as $t \rightarrow \infty$. In this section we build a formalism that can be used to quantify the amount of *long-term information* stored by an RNN; how this amount of information changes with time; and, how the information is related to the smoothness of the cost function.

Assume that at time t the system state \mathbf{x}_t is distributed according to $p_t(\mathbf{x}_t)$. The entropy associated with this probability distribution provides a way of quantifying how much information measuring the state would convey. For the set Ω_x , the entropy can be computed as:

$$H_t = - \int_{\Omega_x} p_t(\mathbf{x}_t) \log p_t(\mathbf{x}_t) d\mathbf{x}_t. \quad (7)$$

Applying the change of variable $\mathbf{x}_{t+1} = \mathbf{f}(\mathbf{x}_t, \mathbf{u}_t; \boldsymbol{\theta})$ we get:⁴

$$\begin{aligned} H_t &= - \int_{\mathbf{f}(\Omega_x, \mathbf{u}_t; \boldsymbol{\theta})} p_{t+1}(\mathbf{x}_{t+1}) \log \left(p_{t+1}(\mathbf{x}_{t+1}) \left| \det \frac{\partial \mathbf{x}_{t+1}}{\partial \mathbf{x}_t} \right| \right) d\mathbf{x}_{t+1} \\ &= H_{t+1} - \int_{\mathbf{f}(\Omega_x, \mathbf{u}_t; \boldsymbol{\theta})} p_{t+1}(\mathbf{x}_{t+1}) \log \left(\left| \det \frac{\partial \mathbf{x}_{t+1}}{\partial \mathbf{x}_t} \right| \right) d\mathbf{x}_{t+1}, \end{aligned}$$

where $\frac{\partial \mathbf{x}_{t+1}}{\partial \mathbf{x}_t}$ is the Jacobian matrix of $\mathbf{f}(\cdot, \mathbf{u}_t; \boldsymbol{\theta})$. Using Hadarmard's inequality:

$$\log \left| \det \frac{\partial \mathbf{x}_{t+1}}{\partial \mathbf{x}_t} \right| \leq \sum_{i=1}^{N_x} \log \|\mathbf{v}_i\|_2, \quad (8)$$

where \mathbf{v}_i is the i -th column of the Jacobian matrix and $\log \|\mathbf{v}_i\|_2 \leq \log \left\| \frac{\partial \mathbf{x}_{t+1}}{\partial \mathbf{x}_t} \right\|_2 \leq \log L_f$. Hence, we have that

$$H_t + N_x \log L_f \leq H_{t+1}. \quad (9)$$

This bound is illustrated in Figure 2 and shows that:

- for a system with $L_f < 1$ (e.g. a contractive system) the entropy might decay over time towards zero. The larger L_f , the slower the decay of information retention can be. For a contractive system all the trajectories will converge to a fixed point. In this case the distribution $p_t(x_t)$ will tend towards a discrete distribution with only one point mass at the fixed point, and thus zero entropy;
- for a system with $L_f = 1$ (e.g. a periodic oscillator), the entropy can stay constant if the bound in (9) is tight. This means that such a system retains information;
- for a system with $L_f > 1$, the amount of entropy increases with time.

Combining these results with those in Theorem 1 suggests that there is a trade-off between the smoothness of the cost function and retention of information. The smaller L_f , the less intricate the cost function, but when $L_f < 1$, information is gradually lost.

⁴An implicit assumption here is that $\mathbf{f}(\cdot, \mathbf{u}_t; \boldsymbol{\theta})$ is a 1-1 continuous differentiable map (cf. theorems 3-13 and 3-14 from [20]).

5 Numerical examples

In this section, we study the properties of the cost function and its relation to the attractors of the RNN. We consider two different tasks.⁵

Classification of symbols according to few relevant, widely separated, symbols. This artificial task was originally described in [12] and requires the neural network to retain information for long periods of time. For this problem, the sequence contains categorical values $\{p, q, a, b, c, d\}$. The symbols $\{a, b, c, d\}$ act as distractors and are not relevant to the task. Instead, the relevant symbols are picked from $\{p, q\}$ appearing only twice in the sequence, at positions t_1 and t_2 . The neural network’s task is to classify the sequence according to which relevant symbols appear and in what order. The four possible classes are $\{(p, p), (p, q), (q, p), (q, q)\}$.

Word language modeling. The Wikitext-2 data set contains 600 Wikipedia articles for training (2,088,628 tokens), 60 articles for validation (217,646 tokens), and 60 articles for testing (245,569 tokens) [21]. The data set has a vocabulary of 33,278 distinct tokens. The goal is to predict the next token in the article given the previous tokens. The state-of-the-art result for the Wikitext-2 data set when not extending the training set is a perplexity on the test set of 39.14 [22]. With our LSTM model implementation, we obtain a perplexity of 106, which is close to other results reported in the literature (i.e. 99.3 obtained for a standard LSTM model in [23]).

Details about the tasks and the models used are reported in Appendix A.

The artificial task, for which long term memory is strictly required for good performance, behaves significantly different compared to the language modeling task involving real data. We focus on three aspects: performance evolution along the epochs, cost function landscape and attractors (i.e. fixed points, periodic dynamics and chaotic behavior).

For the artificial task, the success of training the LSTM to such a task is highly dependent on the initial conditions. For different random initial values of the weights, the training procedure can converge to solutions that have extremely different properties. While, for some initial conditions, an accuracy around 100% is obtained both on training and validation data. In other instances, the accuracy is above 90% on the training set but below 25% on the validation set, i.e. the classifier is no better than random guessing among the 4 possible classes. The convergence toward the solution for these two different scenarios is displayed in Figure 3. In both cases the cost function is intricate and full of local minima as shown in Figure 4. The bifurcation diagram goes from simple fixed points to more complicated attractors as shown in Figure 5. The figure shows the final values of the first output of the network for different initial conditions and when fed with a fixed constant input. In the two top figures, the constant input corresponds to a single non-distractor symbol, whereas in the bottom figure, a distractor symbol is used. In the good performance scenario, the first output converges to a fixed value when the network is fed with a non-distractor symbol (two top figures), whereas the network provides distinct output values when fed with a distractor symbol (bottom figure). In the bad performance scenario, the network provides distinct output values in all cases for parameter values between $\theta^{(\text{init})}$ and $\theta^{(\text{final})}$, i.e. $0 \leq s \leq 1$.

For the word language modeling problem the cost function is well behaved and smooth close the solution. The bifurcation diagram indicates only simple fixed points and the convergence toward the final solution is smooth and well behaved (see Figure 6). This seems to suggest that long term memory is not needed for this task. This is in agreement with results from [16] where truncating RNNs on language model examples has little effect on the performance.

6 Related work

Understanding RNNs by exploring tools from dynamical systems theory is a common approach. It has been speculated that bifurcations might cause the difficulties and jumps in the cost function [14]. The work in [11] formulates the hypothesis that when gradients explode, they do so in some specific direction, creating *walls* of high curvature. The major conceptual difference between our work and that of [14] and [11] is that we, unlike them, advocate that the erratic behavior of the cost function is not limited to boundaries and bifurcation points, but rather span through *entire regions* of the parameter space.

⁵The code for reproducing the experiments will be released upon publication.

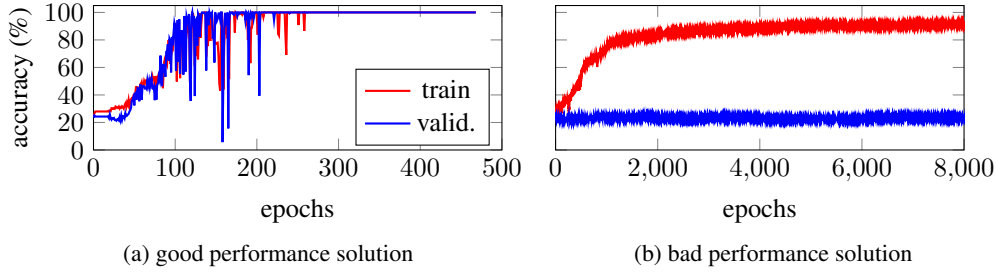


Figure 3: (**widely separated symbols**) Accuracy on training and validation data for two different training scenarios. In (a), the optimization procedure abruptly finds a solution that has good accuracy on both training and validation. In (b), the convergence is slow and steady towards a solution that has good accuracy on the training set (above 90%) but is no better than random guessing on the validation set.

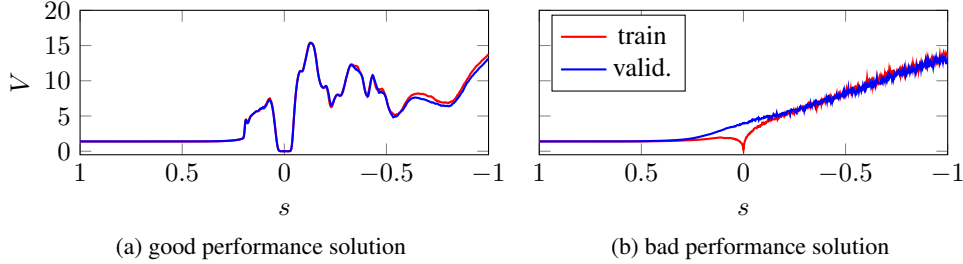


Figure 4: (**widely separated symbols**) Cost function on training for LSTM models with parameter vectors $\theta(s) = s\theta^{(\text{init})} + (1 - s)\theta^{(\text{final})}$, where $\theta^{(\text{init})}$ is the initial parameter vector used to start the optimization, and $\theta^{(\text{final})}$ is the final estimate of the training procedure. In the good performance solution scenario, the network is able to retain long-term information. At the same time, the cost function has several close local minima around the final estimate ($s = 0$) which might make the problem significantly harder. In the bad performance solution, the network does not retain the required long-term information: the cost function has a local minimum on the training data that disappears on the validation set.

Like [9, 10] we also present a trade-off that arises when training RNNs, while [9, 10] point to the trade-off between efficient learning and retaining information robustly in the presence of noise, we instead expose the trade-off between long-term memory and smoothness of the cost function.

Necessary conditions for exploding gradients to appear are also provided in [11]. Their result can be understood as a special case of Theorem 1 and is limited to a single layer of vanilla RNN. By constraining the results to this vanilla case, they do not cover interesting nonlinear behaviors, such as periodic behavior and strange attractors, that are studied here. Our results are also more general, because we include bounds on second order derivatives.

The work in [15] presents a neural network without chaotic behavior. The results presented here, for which the chaotic behavior of LSTMs yield regions in the parameter space where the cost function is highly intricate, densely populated by local minimums and with exploding gradients, is a strong suggestion that this is indeed an interesting line of research that deserves to be further explored.

It has previously [16] been shown that contractive RNNs can be truncated with arbitrarily small effect on both training and prediction. And, hence, contractive RNNs are not significantly different to feedforward networks. However, when restricted to contractive models, RNNs lose the ability to represent several very interesting and relevant dynamical behaviors, such as limit cycles and multiple fixed points. The work in [24] gives examples of recurrent neural networks that do manage to capture some of these rich nonlinear dynamics and provides some tools to help extract dynamic information from the model. These rich dynamics are non-contractive and constitute a good example of what can be achieved in cases for which the training difficulties presented here are overcome.

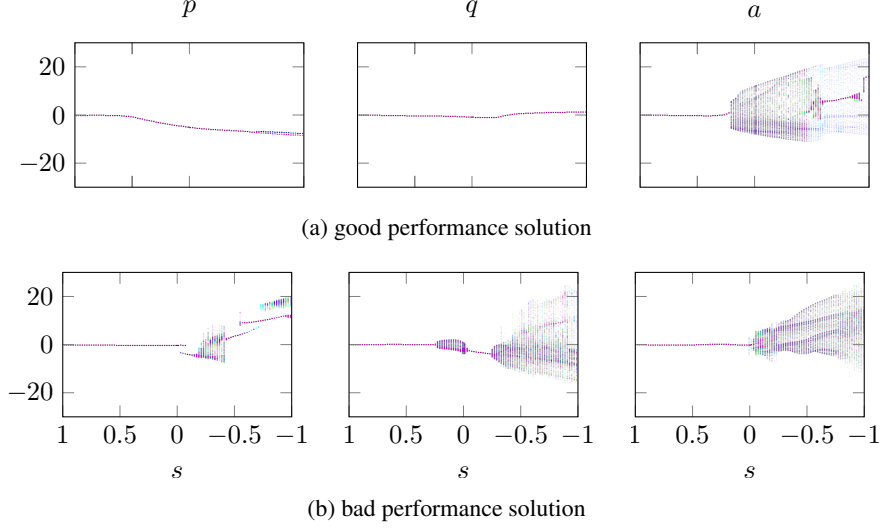


Figure 5: **(widely separated symbols)** Bifurcation diagrams showing the final values of the first output of the network for different initial conditions and when fed with a fixed constant input. In the two leftmost figures, the constant input corresponds to a single non-distractor symbol (p or q), whereas in the rightmost figures, the distractor symbol a is used as input. In the good performance solution scenario, the output converges to a fixed point when the network is fed with a constant non-distractor symbol, whereas the network converge to a periodic or chaotic attractor when fed with a distractor symbol.

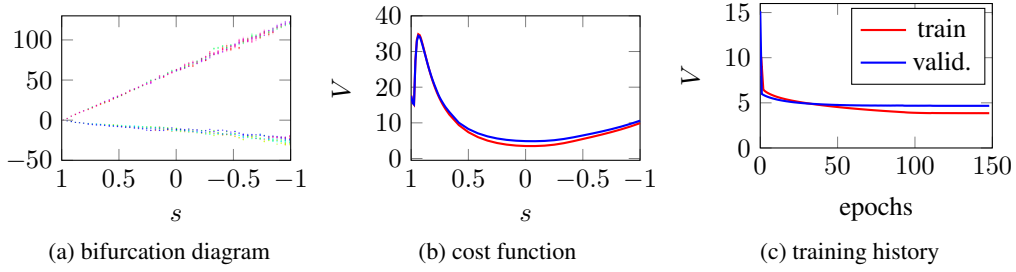


Figure 6: **(wikitext-2)** (a) Bifurcation diagram; (b) Cost function in a straight line; (c) cost function during training. For generating (a) and (b) we use a LSTM models with parameter vectors $\theta(s) = s\theta^{(\text{init})} + (1 - s)\theta^{(\text{final})}$, where $\theta^{(\text{init})}$ is the initial parameter vector used to start the optimization, and $\theta^{(\text{final})}$ is the final estimate of the training procedure.

The notion of using entropy for a dynamical system is not new. One classical definition is that of the Kolmogorov-Sinai entropy [25] which is related to how uncertainty (and information) increase with time in a chaotic attractor. However, this definition cannot be applied for regions of the parameter space that do not preserve volume. The definition presented in Section 4 serves our purpose better, since it does not introduce such restrictions.

7 Conclusion

RNNs represents a more general class of models than feedforward networks. The fact that RNN architectures are gradually loosing ground to the advantage of high performance feedforward architectures [1, 2] on sequence learning tasks, is a clear indication that computational limitations, that is, difficulties in the optimization and regularization are preventing the extra flexibility allowed by these models to yield the best possible performance. We believe that theoretical understanding of these networks might help overcome these challenges.

In this sense, the insight provided here might be used for the design of new regularization techniques and optimization algorithms that might help to properly explore challenging and interesting regions of the RNN parameter space. These regions are challenging to explore, due to their proximity to regions with very high Lipschitz constants, but they are at the same time very interesting because of the possibility of long-term memory behavior.

Acknowledgments

We thank Carl Jidling and Manoel Horta Ribeiro for thoughtful comments and suggestions. This work has been supported by the Brazilian agencies *CAPES - Coordenação de Aperfeiçoamento de Pessoal de Nível Superior* (Finance Code: 001), *CNPq - Conselho Nacional de Desenvolvimento Científico e Tecnológico* (contract number: 302079/2011-4, 200931/2018-0 and 142211/2018-4) and *FAPEMIG - Fundação de Amparo à Pesquisa do Estado de Minas Gerais* (contract number: TEC 1217/98), by the Swedish Research Council (VR) via the projects *NewLEADS – New Directions in Learning Dynamical Systems* (contract number: 621-2016-06079) and *Learning flexible models for nonlinear dynamics* (contract number: 2017-03807), and by the Swedish Foundation for Strategic Research (SSF) via the project *ASSEMBLE* (contract number: RIT15-0012)

References

- [1] A. Vaswani, N. Shazeer, N. Parmar, J. Uszkoreit, L. Jones, A. N. Gomez, Ł. Kaiser, and I. Polosukhin, “Attention is All you Need,” in *Advances in Neural Information Processing Systems 30* (I. Guyon, U. V. Luxburg, S. Bengio, H. Wallach, R. Fergus, S. Vishwanathan, and R. Garnett, eds.), pp. 5998–6008, Curran Associates, Inc., 2017.
- [2] S. Bai, J. Z. Kolter, and V. Koltun, “An Empirical Evaluation of Generic Convolutional and Recurrent Networks for Sequence Modeling,” p. 14, 2018.
- [3] A. van den Oord, S. Dieleman, H. Zen, K. Simonyan, O. Vinyals, A. Graves, N. Kalchbrenner, A. Senior, and K. Kavukcuoglu, “WaveNet: A Generative Model for Raw Audio,” *arXiv:1609.03499 [cs]*, Sept. 2016.
- [4] Y. N. Dauphin, A. Fan, M. Auli, and D. Grangier, “Language modeling with gated convolutional networks,” in *Proceedings of the 34th International Conference on Machine Learning-Volume 70*, pp. 933–941, JMLR.org, 2017.
- [5] A. Radford, K. Narasimhan, T. Salimans, and I. Sutskever, “Improving Language Understanding by Generative Pre-Training,” p. 12, 2018.
- [6] A. Radford, J. Wu, R. Child, D. Luan, D. Amodei, and I. Sutskever, “Language Models are Unsupervised Multitask Learners,” p. 24, 2019.
- [7] N. Kalchbrenner, L. Espeholt, K. Simonyan, A. van den Oord, A. Graves, and K. Kavukcuoglu, “Neural Machine Translation in Linear Time,” *arXiv:1610.10099 [cs]*, Oct. 2016.
- [8] J. Gehring, M. Auli, D. Grangier, and Y. Dauphin, “A Convolutional Encoder Model for Neural Machine Translation,” in *Proceedings of the 55th Annual Meeting of the Association for Computational Linguistics (Volume 1: Long Papers)*, vol. 1, pp. 123–135, 2017.
- [9] Y. Bengio, P. Frasconi, and P. Simard, “The problem of learning long-term dependencies in recurrent networks,” in *IEEE International Conference on Neural Networks*, pp. 1183–1188 vol.3, Mar. 1993.
- [10] Y. Bengio, P. Simard, and P. Frasconi, “Learning long-term dependencies with gradient descent is difficult,” *IEEE Transactions on Neural Networks*, vol. 5, pp. 157–166, Mar. 1994.
- [11] R. Pascanu, T. Mikolov, and Y. Bengio, “On the Difficulty of Training Recurrent Neural Networks,” in *Proceedings of the 30th International Conference on International Conference on Machine Learning - Volume 28, ICML’13*, pp. III–1310–III–1318, JMLR.org, 2013.
- [12] S. Hochreiter and J. Schmidhuber, “Long short-term memory,” *Neural computation*, vol. 9, no. 8, pp. 1735–1780, 1997.
- [13] J. Chung, C. Gulcehre, K. Cho, and Y. Bengio, “Empirical Evaluation of Gated Recurrent Neural Networks on Sequence Modeling,” *arXiv:1412.3555 [cs]*, Dec. 2014.
- [14] K. Doya, “Bifurcations of Recurrent Neural Networks in Gradient Descent Learning,” 1993.

- [15] T. Laurent and J. von Brecht, “A recurrent neural network without chaos,” *arXiv:1612.06212 [cs]*, Dec. 2016.
- [16] J. Miller and M. Hardt, “When Recurrent Models Don’t Need To Be Recurrent,” *arXiv:1805.10369 [cs, stat]*, May 2018.
- [17] Y. Nesterov, *Introductory Lectures On Convex Programming*. 1998.
- [18] A. H. Ribeiro, K. Tiels, J. Umenberger, T. B. Schön, and L. A. Aguirre, “On the Smoothness of Nonlinear System Identification,” *arXiv:1905.00820 [cs, math]*, May 2019.
- [19] W. Rudin, *Principles of Mathematical Analysis*. International Series in Pure and Applied Mathematics, McGraw-Hill, 1964. 00000.
- [20] M. Spivak, *Calculus on Manifolds: A Modern Approach to Classical Theorems of Advanced Calculus*. Mathematics Monograph Series, Cambridge, Mass: Perseus Books, 1998.
- [21] S. Merity, C. Xiong, J. Bradbury, and R. Socher, “Pointer sentinel mixture models,” *arXiv:1609.07843v1*, 2016.
- [22] C. Gong, D. He, X. Tan, T. Qin, L. Wang, and T.-Y. Liu, “Frage: Frequency-agnostic word representation,” *arXiv:1809.06858v1*, 2018.
- [23] N. U. Edouard Grave, Armand Joulin, “Improving neural language models with a continuous cache,” in *International Conference on Learning Representations*, 2017.
- [24] D. Sussillo and O. Barak, “Opening the Black Box: Low-Dimensional Dynamics in High-Dimensional Recurrent Neural Networks,” *Neural Computation*, vol. 25, pp. 626–649, Mar. 2013.
- [25] Y. G. Sinai, “On the notion of entropy of a dynamical system,” in *Dokl. Akad. Nauk. SSSR*, vol. 124, p. 768, 1959.

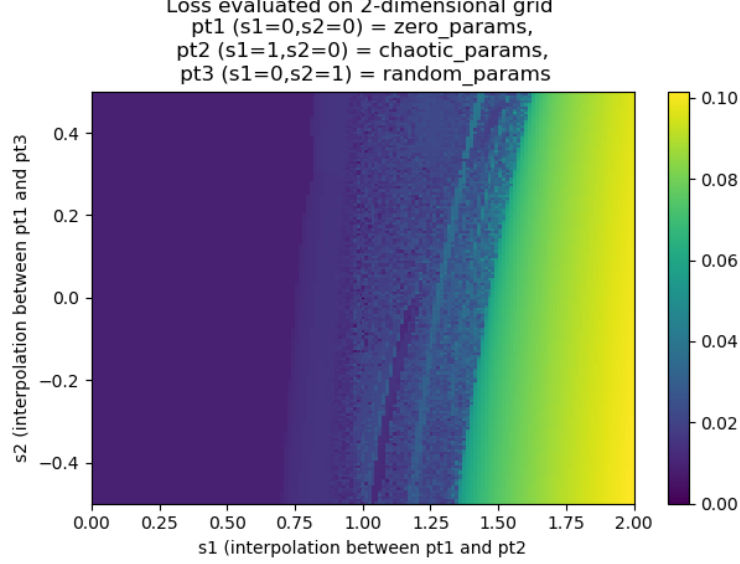


Figure 7: **(Chaotic LSTM)** Mean-square cost function (2) for LSTM models with parameter vectors $\theta(s_1, s_2) = s_1\theta_{\text{true}} + s_2\theta_{\text{random}}$.

A Full description of numerical examples

A.1 Chaotic LSTM

An LSTM with zero input and without bias terms is considered:

$$c_t = \underbrace{\sigma(W_{\text{hf}}h_{t-1})}_{\text{forget gate}} * c_{t-1} + \underbrace{\sigma(W_{\text{hi}}h_{t-1})}_{\text{input gate}} * \underbrace{\tanh(W_{\text{hg}}h_{t-1})}_{\text{cell gate}} \quad (10)$$

$$h_t = \underbrace{\sigma(W_{\text{ho}}h_{t-1})}_{\text{output gate}} * \tanh(c_t). \quad (11)$$

The sigmoids $\sigma(\cdot)$ and hyperbolic tangents $\tanh(\cdot)$ operate element-wise. The symbol $*$ indicates an element-wise product. The hidden and cell state have initial conditions $h_0 = c_0 = [0.5 \ 0.5]^T$. The hidden state h_t is also the output of the model. The weight matrices are put equal to $W_{\text{hi}} = \begin{bmatrix} -1 & 4 \\ -3 & -2 \end{bmatrix}$, $W_{\text{hf}} = \begin{bmatrix} -2 & 6 \\ 0 & -6 \end{bmatrix}$, $W_{\text{hg}} = \begin{bmatrix} -1 & -6 \\ 6 & -9 \end{bmatrix}$, and $W_{\text{ho}} = \begin{bmatrix} 4 & 1 \\ -9 & 7 \end{bmatrix}$ to generate the data. The values in the weight matrices are stacked on top of each other in a parameter vector θ_{true} .

Figure 7 shows the mean-square loss evaluated on data generated by the same LSTM model with the same initial conditions, but with different parameter values. A two-dimensional grid of parameter values $\theta(s_1, s_2)$ is used with values interpolated (and extrapolated) between θ_{true} , zero parameter values, and a randomly chosen parameter vector θ_{random} , i.e. in this case, $\theta(s_1, s_2) = s_1\theta_{\text{true}} + s_2\theta_{\text{random}}$. Again, the region in parameter space around θ_{true} is intricate. There is an entire region where the cost function is intricate and has many neighboring local minima.

A.2 Widely separated symbols

In this experiment, we consider 1000 sequences for training the model. Each sequence with $T = 150$ symbols represented one-hot encoding. The symbols are chosen from a set of four distractor symbols $\{a, b, c, d\}$. At two randomly chosen positions $t_1 \in [10, 19]$ and $t_2 \in [40, 49]$, the distractor symbols are replaced by a symbol randomly chosen from the set $\{p, q\}$ of non-distractor symbols. The goal is to classify the sequence as $\{(p, p), (p, q), (q, p), (q, q)\}$ depending on which non-distractor symbols appear in the sequence and in which order. The validation set consists of another 1,000 of these sequences.

We trained an LSTM model with hidden size 50, followed by a softmax layer that outputs probabilities for the four different classes $\{(p, p), (p, q), (q, p), (q, q)\}$. The model is trained using ADAM with betas (0.9, 0.999)

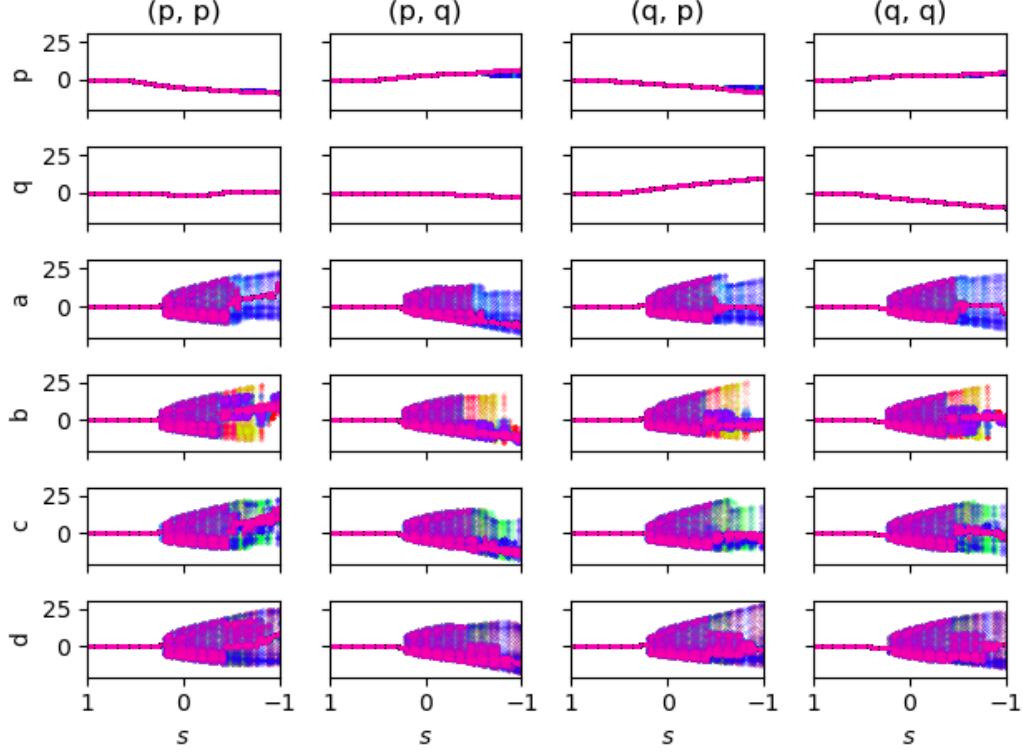


Figure 8: **(Widely separated symbols)** Bifurcation plot for all possible combinations of input and output (good performance scenario). Each row corresponds to a constant input with a fixed symbol (indicated at the left). Each column corresponds to one output class (indicated at the top). Different colors correspond to attractors resulting from different initial conditions.

and a learning rate starts at 10^{-3} and is reduced by a factor 10 at epochs 500, 1000, 2000 epochs. The gradient norm is clipped when it exceeds 0.25. The batch size is 100.

A.3 Word language modeling

The Wikitext-2 data set contains 600 Wikipedia articles for training (having 2,088,628 tokens), 60 articles for validation (having 217,646 tokens), and 60 articles for testing (having 245,569 tokens) [21]. The data set has a vocabulary of 33,278 tokens. Given the previous tokens, the task is to predict the next token in the article.

We trained a model that consists of an embedding layer outputting a size 800 vector to an LSTM with hidden size 800, followed by a softmax decoder layer that outputs probabilities for each token in the vocabulary. The last layer and the embedding have tied layers. A dropout layer is included before and after the LSTM layer with dropout rate 0.5. The models are trained and evaluated using a cross-entropy loss. The model is trained using ADAM with betas (0.9, 0.999) and The learning rate starts at 10^{-3} and is reduced by a factor 10 when the cost function plateaus for more than 7 epochs. The gradient norm is clipped when it exceeds 0.25. The batch size is 100 and the gradient is not backpropagate for a sequence length larger than 80.

B Computing the derivatives

Let the Jacobian matrices of $\mathbf{f}(\mathbf{x}, \mathbf{u}; \boldsymbol{\theta})$ with respect to \mathbf{x} and to $\boldsymbol{\theta}$ evaluated at the point $(\mathbf{x}_t, \mathbf{u}_t; \boldsymbol{\theta})$ be denoted, respectively, as A_t and B_t . Similarly, the Jacobian matrices of $\mathbf{g}(\mathbf{x}, \mathbf{u}_t; \boldsymbol{\theta})$ are denoted as C_t and F_t . A direct application of the chain rule to (1) gives a recursive formula for computing the derivatives of the predicted output in relation to the parameters in the interval $1 \leq t \leq N$:

$$\begin{aligned} D_{t+1} &= A_t D_t + B_t \text{ for } D_0 = \mathbf{0} \\ J_t &= C_t D_t + F_t, \end{aligned} \tag{12}$$

where we denote the Jacobian matrices of $\hat{\mathbf{y}}_t$ and \mathbf{x}_t with respect to $\boldsymbol{\theta}$ respectively as J_t and D_t .

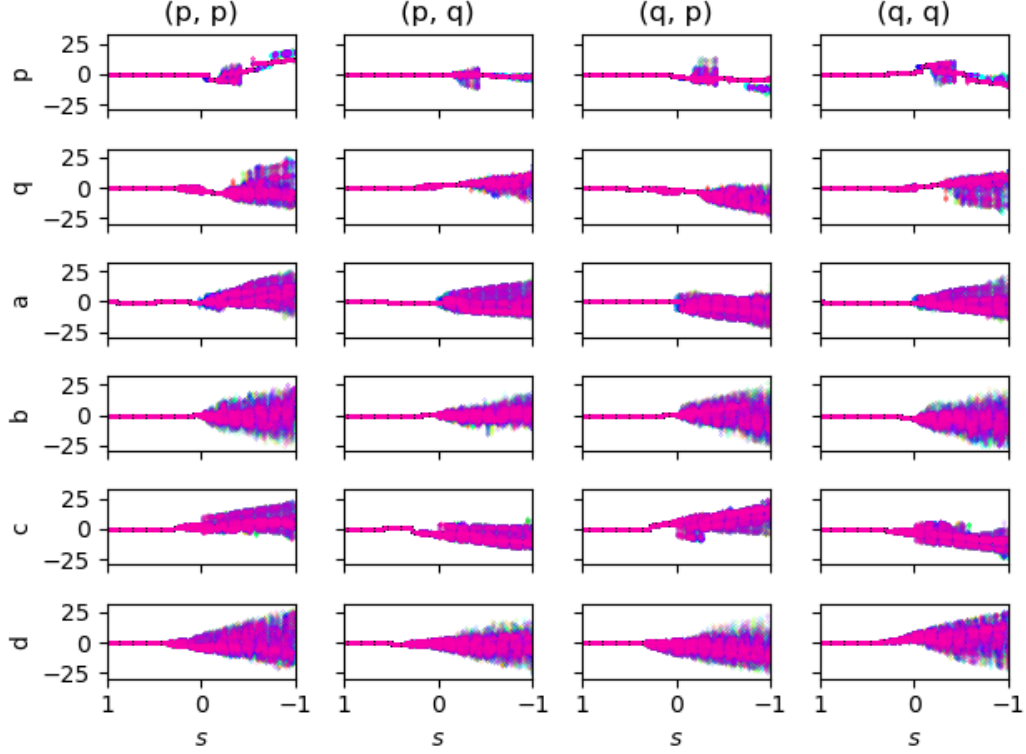


Figure 9: **(Widely separated symbols)** Bifurcation plot for all possible combinations of input and output (bad performance scenario). Each row corresponds to a constant input with a fixed symbol (indicated at the left). Each column corresponds to one output class (indicated at the top). Different colors correspond to attractors resulting from different initial conditions.

For the cost function V defined as in (2), its gradient ∇V is given by:

$$\nabla V = \frac{1}{N} \sum_{t=1}^N J_t l'(\hat{\mathbf{y}}_t, \mathbf{y}_t). \quad (13)$$

where $l'(\hat{\mathbf{y}}_t, \mathbf{y}_t)$ denotes the gradient of the loss function regarding its first argument, evaluated at $(\hat{\mathbf{y}}_t, \mathbf{y}_t)$.

C Proofs

C.1 Preliminary results

Lemma 1. For $i = 1, \dots, n$, let \mathbf{f}_i be a Lipschitz function on Ω with constants L_i . Then,

- a) $\sum_{i=1}^n \mathbf{f}_i$ is also a Lipschitz function on Ω with Lipschitz constant upper bounded by $\sum_{i=1}^n L_i$;
- b) if, additionally, \mathbf{f}_i are bounded by M_i on Ω , then $\prod_{i=1}^n \mathbf{f}_i$ is also a Lipschitz function on Ω with Lipschitz constant upper bounded by $(\sum_{i=1}^n M_1 \cdots M_{i-1} L_i M_{i+1} \cdots M_n)$.

Lemma 2. Let us define the properties:

- 1. $|l(\hat{\mathbf{y}}, \mathbf{y}) - l(\hat{\mathbf{z}}, \mathbf{y})| < (K_1 \|\mathbf{y}\| + K_2 \max(\|\hat{\mathbf{y}}\|, \|\hat{\mathbf{z}}\|)) \|\hat{\mathbf{y}} - \hat{\mathbf{z}}\|$
- 2. $l'(\hat{\mathbf{y}}, \mathbf{y}) = \Psi(\hat{\mathbf{y}}) - K_3 \mathbf{y}$;

where $l'(\hat{\mathbf{y}}, \mathbf{y})$ denotes the first derivative of the loss function regarding its first argument, evaluated at $(\hat{\mathbf{y}}, \mathbf{y})$. There exist constants K_1 , K_2 , and K_3 and a function Ψ that is Lipschitz continuous with constant K_4 and for which Ψ such that these properties hold for both: a) $l(\hat{\mathbf{y}}, \mathbf{y}) = \|\hat{\mathbf{y}} - \mathbf{y}\|^2$; b) $l(\hat{\mathbf{y}}, \mathbf{y}) = -\mathbf{y}^T \log(\sigma(\hat{\mathbf{y}})) - (1 - \mathbf{y})^T \log(1 - \sigma(\hat{\mathbf{y}}))$. In (b), the sigmoid function, $\sigma(x) = \frac{1}{1 + \exp(-x)}$, and the logarithm are evaluated element-wise. We assume in (b) that the elements in \mathbf{y} are either 0 or 1.

Proof. For (a) and (b), property 2 follows from differentiating $l(\hat{\mathbf{y}}, \mathbf{y})$ with regard to its first argument. For (a), $\phi(\hat{\mathbf{y}}) = 2\hat{\mathbf{y}}$ and $K_3 = 2$; for (b), $\phi(\hat{\mathbf{y}}) = \sigma(\hat{\mathbf{y}})$ and $K_3 = 1$.

For loss function (a), property 1 holds because of the following reasoning:

$$\begin{aligned} \|\hat{\mathbf{y}} - \mathbf{y}\|^2 - \|\hat{\mathbf{z}} - \mathbf{y}\|^2 &= \left| \|\hat{\mathbf{y}}\|^2 - \|\hat{\mathbf{z}}\|^2 - 2\mathbf{y}^T (\hat{\mathbf{y}} - \hat{\mathbf{z}}) \right| \\ &\leq \left| (\|\hat{\mathbf{y}}\| - \|\hat{\mathbf{z}}\|) (\|\hat{\mathbf{y}}\| + \|\hat{\mathbf{z}}\|) - 2\mathbf{y}^T (\hat{\mathbf{y}} - \hat{\mathbf{z}}) \right| \\ &\leq (2\|\mathbf{y}\| + 2\max(\|\hat{\mathbf{y}}\|, \|\hat{\mathbf{z}}\|)) \|\hat{\mathbf{y}} - \hat{\mathbf{z}}\| \end{aligned}$$

For loss function (b), let \hat{y} and \hat{z} be two scalar values. Furthermore, consider, without loss of generality, that $\hat{y} \geq \hat{z}$. Then:

$$0 \leq \log(\sigma(\hat{y})) - \log(\sigma(\hat{z})) = (\hat{y} - \hat{z}) - \log\left(\frac{\exp(\hat{y}) + 1}{\exp(\hat{z}) + 1}\right) \leq (\hat{y} - \hat{z}) \quad (14)$$

The first inequality follows from the fact that $\log(\sigma(\cdot))$ is a monotonically increasing function. The last inequality holds because $\log\left(\frac{\exp(\hat{y}) + 1}{\exp(\hat{z}) + 1}\right) \geq 0$. Analogously,

$$0 \leq \log(1 - \sigma(\hat{z})) - \log(1 - \sigma(\hat{y})) = (\hat{y} - \hat{z}) - \log\left(\frac{\exp(-\hat{z}) + 1}{\exp(-\hat{y}) + 1}\right) \leq (\hat{y} - \hat{z}) \quad (15)$$

For $l(\mathbf{y}, \hat{\mathbf{y}})$ defined as in (b), it follows from (14), (15), and the fact that \mathbf{y} contains only values in the set $\{0, 1\}$, that:

$$|l(\hat{\mathbf{y}}, \mathbf{y}) - l(\hat{\mathbf{z}}, \mathbf{y})| \leq \|\hat{\mathbf{y}} - \hat{\mathbf{z}}\|_1 \leq \sqrt{N_y} \|\hat{\mathbf{y}} - \hat{\mathbf{z}}\|_2 \quad (16)$$

where $\|\cdot\|_1$ and $\|\cdot\|_2$ denote l_1 and l_2 norm of a vector and N_y is the number of outputs. \square

C.2 Proof of Theorem 1 (a)

Assume two different trajectories resulting from simulating the system (1) with parameters and initial conditions $(\mathbf{x}_0, \boldsymbol{\theta})$ and $(\mathbf{w}_0, \boldsymbol{\phi})$, respectively. We denote the corresponding trajectories by \mathbf{x} and \mathbf{w} . Let us call:

$$\|\Delta\hat{\mathbf{y}}_t\| = \|\mathbf{g}(\mathbf{x}_t, \mathbf{u}_t; \boldsymbol{\theta}) - \mathbf{g}(\mathbf{w}_t, \mathbf{u}_t; \boldsymbol{\phi})\|. \quad (17)$$

Because \mathbf{f} and \mathbf{g} are Lipschitz in $(\mathbf{x}, \boldsymbol{\theta})$ we have:

$$\begin{aligned} \|\mathbf{f}(\mathbf{x}, \mathbf{u}_t, \boldsymbol{\theta}) - \mathbf{f}(\mathbf{w}, \mathbf{u}_t, \boldsymbol{\phi})\|^2 &\leq L_f^2 (\|\mathbf{x} - \mathbf{w}\|^2 + \|\boldsymbol{\theta} - \boldsymbol{\phi}\|^2), \\ \|\mathbf{g}(\mathbf{x}, \mathbf{u}_t, \boldsymbol{\theta}) - \mathbf{g}(\mathbf{w}, \mathbf{u}_t, \boldsymbol{\phi})\|^2 &\leq L_g^2 (\|\mathbf{x} - \mathbf{w}\|^2 + \|\boldsymbol{\theta} - \boldsymbol{\phi}\|^2), \end{aligned}$$

for all $(\mathbf{x}, \mathbf{u}_t, \boldsymbol{\theta})$ and $(\mathbf{w}, \mathbf{u}_t, \boldsymbol{\phi})$ in $(\Omega_{\mathbf{x}}, \Omega_{\mathbf{u}}, \Omega_{\boldsymbol{\theta}})$. Applying these relations recursively we get that:

$$\|\Delta\hat{\mathbf{y}}_t\|^2 \leq L_g^2 L_f^{2t} \|\mathbf{x}_0 - \mathbf{w}_0\|^2 + L_g^2 \left(\sum_{\ell=0}^t L_f^{2\ell} \right) \|\boldsymbol{\theta} - \boldsymbol{\phi}\|^2.$$

Since L_f is positive, the constant multiplying the second term in the above equation is always larger than the constant multiplying the first term. Hence, taking the square root on both sides of the above inequality and after simple manipulations, we get:

$$\|\Delta\hat{\mathbf{y}}_t\| \leq L_g S(t) \|\boldsymbol{\theta}, \mathbf{x}_0\|^T - [\boldsymbol{\phi}, \mathbf{w}_0]^T. \quad (18)$$

where:

$$S(t) = \sqrt{\sum_{\ell=0}^t L_f^{2\ell}} = \begin{cases} \sqrt{t+1} & \text{if } L_f = 1 \\ \sqrt{\frac{L_f^{2t+2}-1}{L_f^2-1}} & \text{if } L_f \neq 1. \end{cases} \quad (19)$$

Since Ω is compact and $\hat{\mathbf{y}}_t$ is a (Lipschitz) continuous function of the parameters and initial conditions, then $\hat{\mathbf{y}}_t$ is bounded in Ω , i.e. $\|\hat{\mathbf{y}}_t\| \leq M(t)$. And, it follows from (18) and from the existence of an invariant set⁶ in Ω that $M(t) = \mathcal{O}(S(t))$.

⁶There are multiple ways to guarantee the invariant set premise will hold, but a very simple way is to just choose \mathbf{f} such that $\mathbf{f}(\mathbf{0}, \mathbf{u}_t; \mathbf{0}) = \mathbf{0}$. In this case, $\{\mathbf{0}\}$ is an invariant set and if $\Omega_{\boldsymbol{\theta}}$ contains this point the premise is satisfied. For this specific case, one can just choose $[\boldsymbol{\phi}, \mathbf{w}_0] = \mathbf{0}$ and it follows from (18) that $\|\hat{\mathbf{y}}_t\| \leq L_g S(t) \|\boldsymbol{\theta}, \mathbf{x}_0\| = \mathcal{O}(S(t))$. The more general case, for any invariant set, follows from a similar deduction.

The following inequality follows from (2), and from property 1 from Lemma 2:

$$|V(\boldsymbol{\theta}, \mathbf{x}_0) - V(\boldsymbol{\phi}, \mathbf{w}_0)| \leq \frac{1}{N} \sum_{t=1}^N (K_1 L_y + K_2 M(t)) \|\Delta \hat{\mathbf{y}}_t\|, \quad (20)$$

where $L_y = \max_{1 \leq t \leq N} \|\mathbf{y}_t\|$. And, by putting together (20) and (18):

$$|V(\boldsymbol{\theta}, \mathbf{x}_0) - V(\boldsymbol{\phi}, \mathbf{w}_0)| \leq L_{V_1} \left\| [\mathbf{x}_0, \boldsymbol{\theta}]^T - [\mathbf{w}_0, \boldsymbol{\phi}]^T \right\|,$$

for $L_V = \left(\frac{L_g}{N} \sum_{t=1}^N (K_1 L_y + K_2 M(t)) S(t) \right)$. The asymptotic analysis of this expression with regard to N yields (4).

C.3 Proof of Theorem 1 (b)

It follows from (13), and from property 2 from Lemma 2, that:

$$\|\nabla V(\boldsymbol{\theta}, \mathbf{x}_0) - \nabla V(\boldsymbol{\phi}, \mathbf{w}_0)\| \leq \frac{1}{N} \sum_{t=1}^N K_3 L_y \|\Delta J_t\| + \|\Delta(J_t \Psi(\hat{\mathbf{y}}_t))\|, \quad (21)$$

where we have used the notation ΔJ_t to denote the difference between J_t evaluated at $(\boldsymbol{\theta}, \mathbf{x}_0)$ and $(\boldsymbol{\phi}, \mathbf{w}_0)$. Analogously, $\Delta(J_t \Psi(\hat{\mathbf{y}}_t))$ denotes the difference between $J_t \Psi(\hat{\mathbf{y}}_t)$ evaluated at the two distinct points, where Ψ is the Lipschitz continuous function with constant K_4 defined in Lemma 2.

From equation (12) it follows that:

$$J_t = C_t \sum_{\ell=1}^t \left(\prod_{j=1}^{t-\ell} A_{t-j+1} \right) B_\ell + F_t; \quad (22)$$

Since the Jacobian of \mathbf{f} is Lipschitz with Lipschitz constant L'_f , it follows that:

$$\|\Delta A_j\|^2 \leq (L'_f)^2 (\|\mathbf{x}_j - \mathbf{w}_j\|^2 + \|\boldsymbol{\theta} - \boldsymbol{\phi}\|^2). \quad (23)$$

Using a procedure analogous to the one used to get Equation (18), it follows that:

$$\|\Delta A_j\| \leq L'_f S(j) \|\boldsymbol{\theta}, \mathbf{x}_0\|^T - [\boldsymbol{\phi}, \mathbf{w}_0]^T\|, \quad (24)$$

where $S(j)$ is defined as in (19). An identical formula holds for B_j and a similar formula, replacing L'_f with L'_g , holds for C_j and F_j .

Since \mathbf{f} and \mathbf{g} are Lipschitz with Lipschitz constants L_f and L_g it follows that $\|A_j\| \leq L_f$, $\|B_j\| \leq L_f$, $\|C_j\| \leq L_g$ and $\|F_j\| \leq L_g$. Hence, it follows from (18), (22), (24) and the repetitive application of Lemma 1 that $\|\Delta J_t\|$ and $\|\Delta(J_t \Psi(\hat{\mathbf{y}}_t))\|$ are upper bounded by $\|\boldsymbol{\theta}, \mathbf{x}_0\|^T - [\boldsymbol{\phi}, \mathbf{w}_0]^T\|$ multiplied by the following constants:

$$\begin{aligned} L_{J,t} &= \sum_{\ell=1}^t P(t, \ell) + L'_g S(t); \\ L_{J\hat{\mathbf{y}},t} &= \sum_{\ell=1}^t Q(t, \ell) + T(t) S(t), \end{aligned}$$

where $T(t) = K_4(L'_g M(t) + L_g^2)$ and:

$$\begin{aligned} P(t, \ell) &= L_f^{t-\ell} \left(L_g L'_f \sum_{j=\ell}^t S(j) + L_f L'_g S(t) \right); \\ Q(t, \ell) &= L_f^{t-\ell} \left(K_4 M(t) L_g L'_f \sum_{j=\ell}^t S(j) + L_f T(t) S(t) \right). \end{aligned}$$

Hence,

$$\|\nabla V(\boldsymbol{\theta}, \mathbf{x}_0) - \nabla V(\boldsymbol{\phi}, \mathbf{w}_0)\| \leq L'_V \|\boldsymbol{\theta}, \mathbf{x}_0\|^T - [\boldsymbol{\phi}, \mathbf{w}_0]^T\|,$$

where:

$$L'_V = \frac{1}{N} \sum_{t=1}^N (K_3 L_y L_{J,t} + L_{J\hat{\mathbf{y}},t}).$$

Putting everything together, the asymptotic analysis of L'_V results in (5).